Design of novel circular lattice photonic crystal fiber suitable for transporting 48 OAM modes

Alaaeddine Rjeb[1]*, Habib Fathallah[2], Saleh Chebaane[3], and Mohsen Machhout[1]

1. *Laboratory of Electronic and Microelectronic, Physics Department, Faculty of Sciences of Monastir, University of Monastir, Monastir 5000, Tunisia*
2. *Laboratory of Artificial Intelligence and Data Engineering Applications, Computer Department, Faculty of Sciences of Bizerte, University of Carthage, Bizerte 7000, Tunisia*
3. *Physics Department, College of Science, University of Hai'il, Kingdom of Saudi Arabia*

(Received 15 October 2020; Revised 30 December 2020)

In this paper, we propose and numerically investigate a novel circular lattice photonic crystal fiber (CL-PCF) using controllable GeO_2 doped silica, suitable for modes carrying quantized orbital angular momentum (OAM). Large effective index separations between 25 supported vector modes ($\geq 10^{-4}$) are confirmed over large bandwidth (C+L bands) leading to 48 OAM modes bearing information. The simulations show that the modes in the proposed CL-PCF have good features including low and flat dispersion (within 51.82 ps/km/nm), low confinement loss (lower than 0.002 dB/m), high effective mode area (88.5 μm^2) and low nonlinearity (1.22 $W^{-1}\cdot km^{-1}$). These promising results show that the proposed CL-PCF could be an arguably candidate in fiber-based OAM multiplexing or other applications using OAM states.

Document code: A **Article ID:** 1673-1905(2021)08-0501-6
DOI https://doi.org/10.1007/s11801-021-0158-7

Space division multiplexing (SDM) has gained widespread interest in optical communication based on fibers or in free space optics (FSO)[1]. SDM consists on carrying data on independent paths (channels) to increase the capacity transmission and improve the spectral efficiency. One of the most promising approaches in SDM is the exploitation of orbital angular momentum (OAM) of light as another degree of freedom to encode information[2]. Taking benefit from its inherent orthogonality, its unboundedness, and its unique phase distribution property, OAM has shown a terabit scale in optical fibers based communication as well as FSO link[3,4].

To support robust and high OAM order, many kinds of optical fibers from both categories (conventional fibers and photonics crystal fibers) have been designed. These fibers are known as OAM-fibers or OAM specialty fibers. Examples of conventional OAM-fibers are air core fiber (ACF)[5], ring core fiber (RCF)[6], inverse parabolic graded index fiber (IPGIF)[7], graded index ring core fiber (GIRCF)[8] and inverse raised cosine fibers (IRCF)[9]. On the other hand, photonic crystal fibers (PCF) has shown its design flexibility to guide appropriate OAM modes. With adjustable parameters, PCF can offer more flexible design structures to provide unique fiber properties[10]. Due to that, several kinds of OAM-PCF with various structures (hexagonal, circular, kagome, etc) and materials (As_2S_3, SiO_2, polymer, etc), having promising features have been designed and fabricated. PCFs supporting 1[11], 2[12], 10[13], 12[14], 14[15], 26[16,17], 34[18,19], and 42[20], first order OAM modes have been proposed featuring good transmission properties. The race is still ongoing to increase the number of OAM modes in PCF featuring good transmission proprieties. By analysis of these recent mosaic OAM-PCFs literature, we can synthesize the general requirements in PCF design that ensure good transmission quality of OAM modes in the following five points or guidelines: (1) Fiber index profile that matches the intensity profile of OAM modes; (2) The supported modes belonging to the same OAM mode family should possess a large index separation ($\geq 10^{-4}$) to be free from complex and heavy multiple input multiple output digital signal processing (MIMO DSP) at the receiver side. This is achievable with high material contrast between the fiber core and the cladding. Instead of using SiO_2 as a background material for the PCF-fiber, other available materials could be used such as silicon (Si)[21], As_2S_3[12], and polymer[22]; (3) Large core thickness is required targeting to increase the supported OAM mode number; (4) The excited OAM modes should be of the first order. Hence, it is preferable to avoid exciting the higher radial orders modes because it causes trouble in multiplexing and demultiplexing operations due to the intensity and phase variety distribution; (5) The guided OAM modes would possess good transmission features

* E-mail: alaaeddine.Rjeb@gmail.com

such as low confinement loss, flat dispersion, large effective mode area, and low nonlinear coefficient over a large wavelength range (at least covering C+L bands defined by ITU-T)[17].

Based on the detailed considerations (guidelines) above, in this paper, we propose and numerically examine a new circular lattice photonic crystal fiber (CL-PCF) suitable for transmitting OAM modes. The material and geometrical parameters of the proposed CL-PCF are optimized in order to enhance the number of first order modes excited and allows the material dispersion to be nearly zero. The designed CL-PCF supports in total 25 vector modes equivalent to 48 OAM modes/channels carrying data. The modes' performance metrics including the intermodal separation, the chromatic dispersion, the confinement loss, the effective area, and the nonlinearity are numerically investigated and compared to some recently reported PCFs. The obtained results show that the proposed CL-PCF could be a viable candidate for next SDM applications using OAM modes.

The proposed CL-PCF is shown in Fig.1. The PCF is composed of circular large air hole at the center with radius a, surrounded by small air holes (blue circles) arranged (distributed) into four circular arrays (circular lattice). The size of array-air holes is similar (homogenous) in order to reduce the complexity and simplify the PCF-structure. d_1 is the air holes diameter, d_s is the distance between the center hole and the first air hole ring, and Λ is the distance between two adjacent air holes from the same ring (air hole pitch).

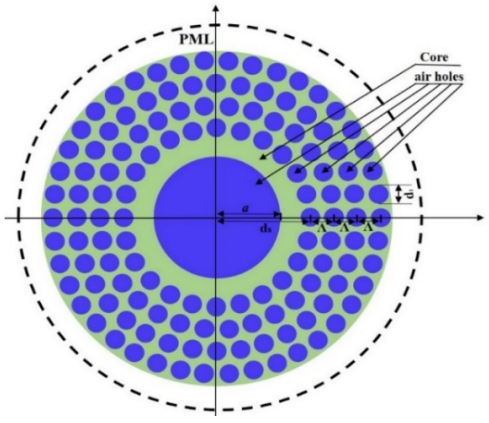

Fig.1 Cross-section and main parameters of the proposed CL-PCF

In this work, we set d_1=1.6 μm, Λ=2 μm (fixed) for reason of brevity and aiming to simplify the present analysis. The former values are selected based on the works reported in Refs.[11—20]. Moreover, a PCF with heterogeneous air hole size and variable core pitch are difficult to be fabricated.

The proposed material background is the germania doped silica (GeO_2-SiO_2), this ensures high refractive index contrast between core and cladding. Moreover, it enhances the effective index separation (Δn_{eff}) between adjacent vector modes (HE and EH) required for the stability of OAM modes and being transparent to couple into undesired LP modes. From polarization maintaining fibers, $\Delta n_{\text{eff}} \geq 10^{-4}$ between supported vector modes, is required to keep OAM modes transmission stability[3]. In addition, GeO_2 doped silica leads to control the dispersion properties of the PCF[23]. The total dispersion is given by[24]:

$$D \approx D_{\text{m}}(\lambda) + D_{\text{w}}(\lambda), \tag{1}$$

where $D_{\text{m}}(\lambda)$ is the material dispersion and $D_{\text{w}}(\lambda)$ is the waveguide dispersion, both given by[21]:

$$D_{\text{m}} = -\frac{\lambda}{c}\frac{\mathrm{d}^2 n}{\mathrm{d}\lambda^2}, \tag{2}$$

$$D_{\text{w}} = -\frac{\lambda}{c}\frac{\mathrm{d}^2 n_{\text{eff}}}{\mathrm{d}\lambda^2}, \tag{3}$$

where λ is the wavelength in vacuum and c is the light velocity in vacuum, n is the material refractive index and n_{eff} is the mode effective index. By controlling the GeO_2 concentration (mol%), the material dispersion can be reduced, more even suppressed at operating wavelength (e.g. λ=1.55 μm). Hence, the total dispersion will be limited to only D_{w}. The refractive indexes $n(\lambda)$ of GeO_2 and SiO_2 are calculated based on seillmeir equations[25]. The refractive index $n(\lambda)$ of the composite material is given by[25]:

$$n^2(\mathrm{GeO_2}-\mathrm{SiO_2}) = 1 - \sum_{i=0}^{3} \frac{\left[SA_i + X(GA_i - SA_i)\right]\lambda^2}{\lambda^2 - \left[Sl_i + X(Gl_i - Sl_i)\right]^2}, \tag{4}$$

where SA, Sl, GA, Gl are the Sellmeier coefficients for the SiO_2 and GeO_2 glasses and X is the doping concentration of GeO_2 (mol%). Based on Eqs.(2) and (4) the material dispersion is given in Fig.2(a). The selected wavelength bands are the entire C+L bands defined by the ITU-T ranging from 1.525 μm to 1.625 μm, which are widely used in optical fiber communication. At λ=1.55 μm, the optimal dispersion D_{m} is (nearly zero) achieved when the doping concentration of GeO_2 (mol%) is X=50%. Hence, with that selected value (X), the final refractive index curve of the composite background material over C+L bands is shown in Fig.2(b) (blue line).

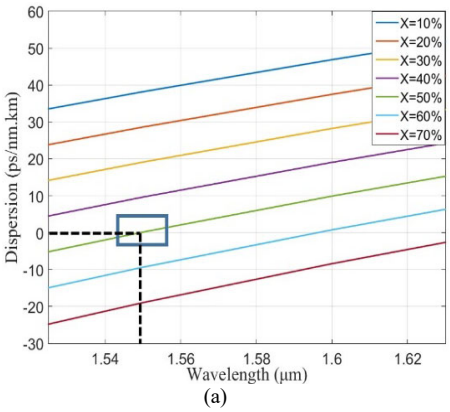

(a)

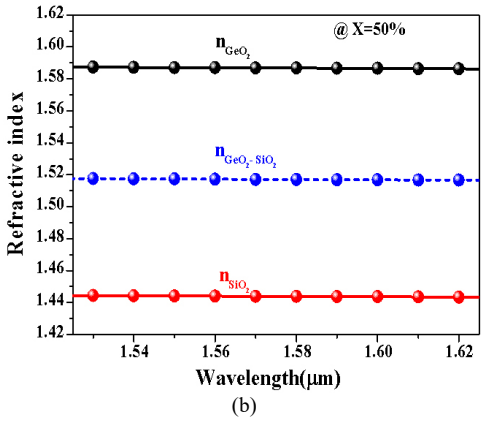

Fig.2 Plots of material dispersion versus wavelength for a GeO_2 doped SiO_2 core PCF with different doping concentrations of GeO_2; (b) Plots of refractive index versus wavelength for silica SiO_2, GeO_2 and GeO_2 doped SiO_2 core with GeO_2 doping concentration of X=50%

The core thickness should be improved with optimization since it simultaneously affects the number of supported modes as well as its orders. Targeting to ensure the exciting of only the first order OAM modes (m=0), we fix the distance between center hole and first array (d_s=8 μm) while we varying the center air hole radius (a). Using finite element method (FEM) mode solver (Comsol multiphysics) at wavelength (λ=1.55 μm), in addition, to perfect matched layer PML to prevent spurious reflections from the numerical boundaries; the resulting modal map versus a (top axis) is presented in Fig.3.

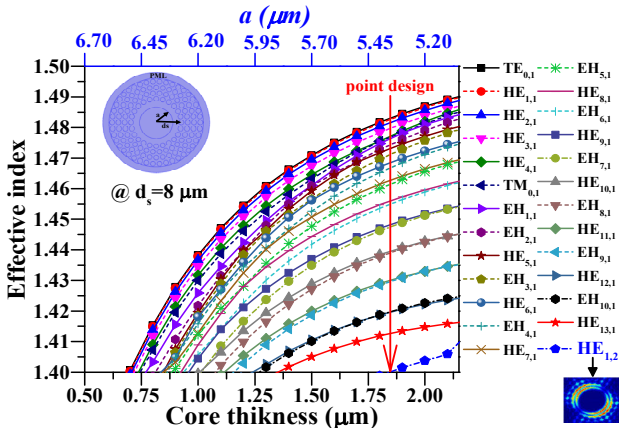

Fig.3 Modal map of the proposed CL-PCF at λ=1.55 μm, d_1=1.6 μm, Λ=2 μm

From that map, the $HE_{1,2}$ (responsible for the second order OAM mode) is excited when the core thickness (bottom axis) is around 1.85 μm. The maximum number of the first order vector modes is 25 including $HE_{l,m}$, $EH_{l,m}$, $TE_{0,m}$ and $TM_{0,m}$. The intensity distributions of all the resulting vector modes are shown in Fig.4.

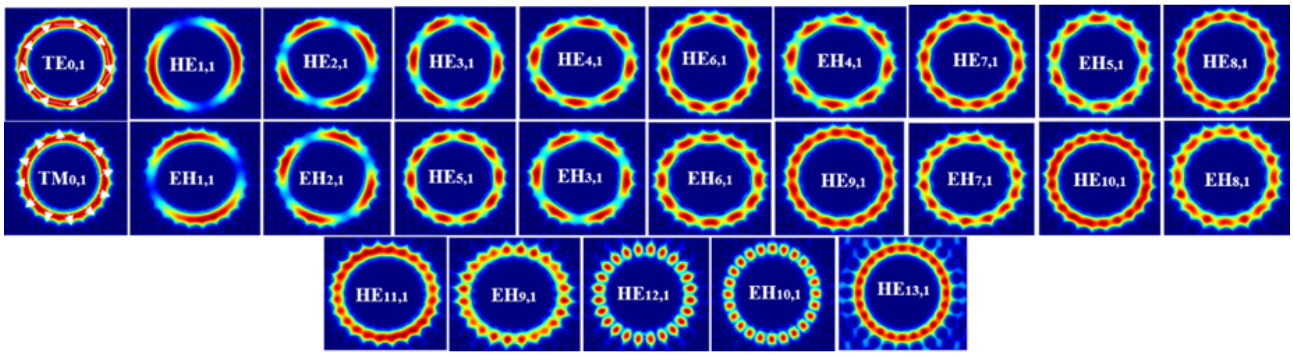

Fig.4 The electric field distributions of all the vector modes in the designed CL-PCF (Arrows indicate the direction of transverse electric field.)

Numerical analysis is carried out using FEM solver (Comsol multiphysics) in order to obtain the electromagnetic field distributions and the effective indices of the supported vector modes in the proposed CL-PCF.

The mode effective indexes as a function of wavelength for different modes are shown in Fig.5(a). The designed PCF supports all the above 25 vector modes over the entire C+L bands. We evaluate the effective index separation (Δn_{eff}) between $HE_{l,m}$ and $EH_{l,m}$ mode belonging the same OAM family (same topological number l) along all the C+L band. The results are highlighting in Fig.5(b). All the Δn_{eff} are up to 10^{-4}, which limits the interaction between vector modes and guarantees the stable transmission of resulting OAM modes.

OAM modes are generating by combining the even and odd modes for each $HE_{l,m}$ and $EH_{l,m}$ eigenmodes with a (π/2) phase shift. The synthesis formulas of OAM modes from fiber cylindrical vector modes are expressed as follows[17]:

$$\mathrm{HE}_{l+1,m}^{\text{even}} \pm \mathrm{i} \times \mathrm{HE}_{l+1,m}^{\text{odd}} = \mathrm{OAM}_{\pm l,m}^{\mathrm{L/R}}, \quad (5.a)$$

$$\mathrm{EH}_{l-1,m}^{\text{even}} \pm \mathrm{i} \times \mathrm{EH}_{l-1,m}^{\text{odd}} = \mathrm{OAM}_{\pm l,m}^{\mathrm{L/R}}, \quad (5.b)$$

where L/R superscript are left (L) or right (R) circular polarization (SAM as spin angular momentum), $\pm l$ subscript refers to the topological charge number, and m is the mode radial index. Interpolating these relations in FEM, the proposed PCF supports in total 48 OAM states along the entire C+L band. The combination between TE and TM modes does not provide OAM modes due to the high separation among their effective indexes but they

are included in our analysis. In addition, usually, the fundamental mode ($OAM_{0,1}$) is not considered as OAM mode due to the plane wave front that possess but it is still an available data channels that carry information in SDM system. Part of spatial-phase distributions of the *x*-component electric field of all the OAM modes are manifested in Fig.6.

We assess the chromatic dispersion of the supported modes in the proposed CL-PCF. By definition, the chromatic dispersion is the spreading of a pulse as it propagates along the fiber which enables performance degradation. The chromatic dispersion is calculated and shown in Fig.7. All the dispersion curves of modes are flat and almost stable over the entire C+L band. Additionally, the dispersions values of HE modes are less than EH modes

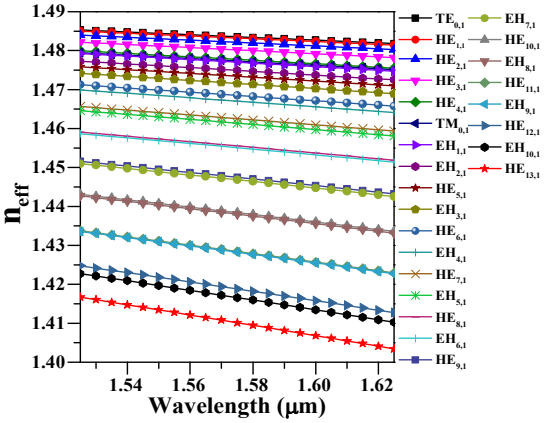

(a)

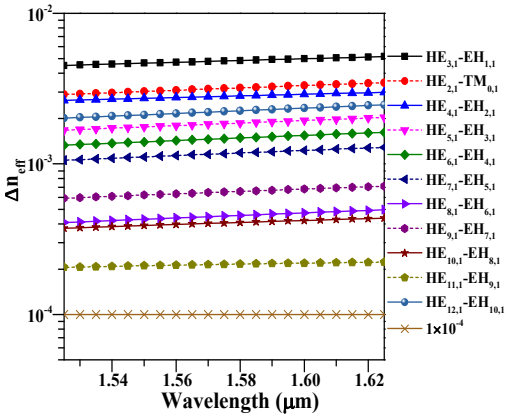

(b)

Fig.5 (a) Effective indices (n_{eff}) as a function of wavelength for different modes; (b) Δn_{eff} between HE and EH modes of the same OAM group along all the C+L band

belonging to the same OAM family. The mode $HE_{13,1}$ has the highest dispersion within (47.72 to 51.82) (ps/km·nm), while the lowest dispersion is for $HE_{1,1}$ valuing around 5.50 (ps/km·nm). These dispersions values are low since they are better than those in Refs.[12] and [20]. In principle, for controlling the chromatic dispersion in PCF, it is preferable to adjust both the air holes diameters (i.e. d_1) and the hole-to-hole spacing (i.e. the pitch Λ). On the other hand, this helps to tailor the dispersion and dispersion slope but it will come at the price of increasing the complexity of fiber fabrication hence, tradeoff designs are required.

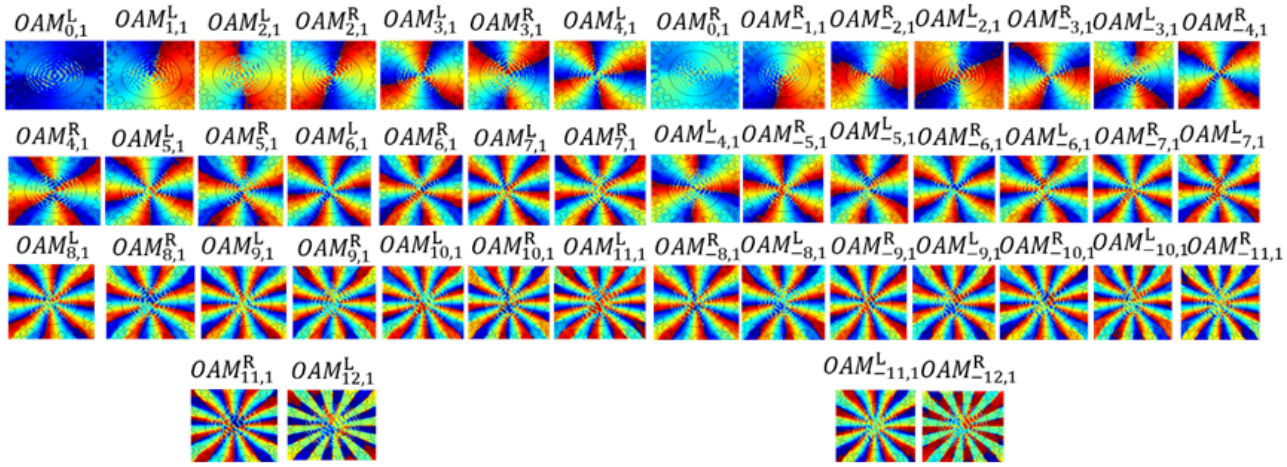

Fig.6 Part of phase plot of all the supported OAM modes in CL-PCF

We evaluate the confinement loss (dB/m) for the proposed CL-PCF structures. The expression of confinement loss is as follows[17]:

$$L = \frac{2\pi}{\lambda}\frac{20}{\ln 10}10^6\,\mathrm{Im}(n_{\mathrm{eff}}), \tag{6}$$

where $\mathrm{Im}(n_{\mathrm{eff}})$ is the imaginary part of mode effective index and λ is the wavelength. The results are plotted in Fig.8. One can see that the confinement loss increases with the increase of mode order. This explained by the more chance for higher modes to leak to the cladding compared with lower order modes. In addition, the confinement loss of HE mode is higher than that of EH mode belonging to the same family. The highest confinement loss is for $HE_{13,1}$ and it is within 0.002 to 0.041 (dB/m) along the C+L bands. This value is clearly less than those in Refs.[17] and [20]. Moreover, these con-

finement loss levels indicate the high purity of generated OAM modes hence leading to long distance OAM mode transmission using the designed CL-PCF.

In this sub-section, we assess the modes effective area (A_{eff}) and the nonlinearity coefficient (γ). Both performance metrics parameters are given by the following expressions[17]:

$$A_{\text{eff}} = \frac{\left\{\iint |E(x,y)| \mathrm{d}x\mathrm{d}y\right\}^2}{\iint |E(x,y)|^4 \mathrm{d}x\mathrm{d}y}, \tag{7}$$

$$\gamma = \frac{2\pi n(\mathrm{GeO_2} - \mathrm{SiO_2})}{\lambda A_{\text{eff}}}, \tag{8}$$

where $E(x,y)$ is the electrical field distribution of the transverse field, and $n_{(\mathrm{GeO2\text{-}SiO2})}$ is the nonlinear index of the composite (GeO_2-SiO_2) calculated as $n_{(\mathrm{GeO2\text{-}SiO2})}$= 2.507+0.505$X$[26]. The A_{eff} and γ are shown in Fig.8(a) and Fig.9(b), respectively.

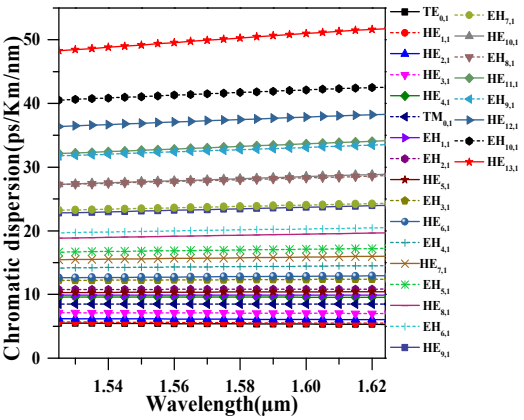

Fig.7 Dispersion as a function of wavelength for different modes in the designed CL-PCF

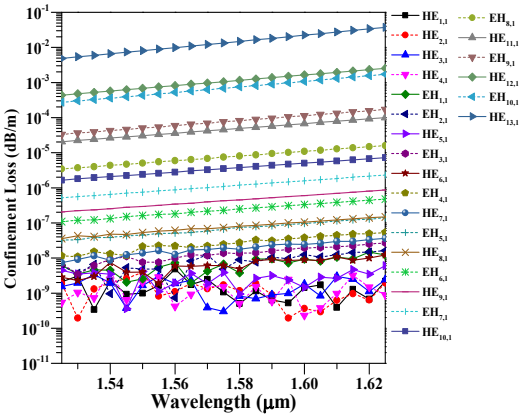

Fig.8 Confinement loss for all the supported modes in the designed PCF along the C+L bands

From Fig.9(a), it is clear that the effective mode area increases slowly with the increasing of wavelength. In addition, it increases with the mode order. Since the nonlinearity is inversely proportional to the effective area we can conclude (also seen in Fig.9(b)) that the nonlinearity decreases with the increase of wavelength and fiber mode order. The maximum effective area is for $HE_{13,1}$ valuing within 78.03—88.65 μm^2 which is equivalent to nonlinearity within 0.93—1.22 W^{-1}·km^{-1} over the entire C+L bands. These levels of nonlinear coefficient are clearly better than those reported in Refs.[17] and [20]. Samely, the nonlinear coeficient can be tailored by varying the cladding parameters including air hole diameters (i.e. d_1) and hole to hole pitch (i.e. Λ).

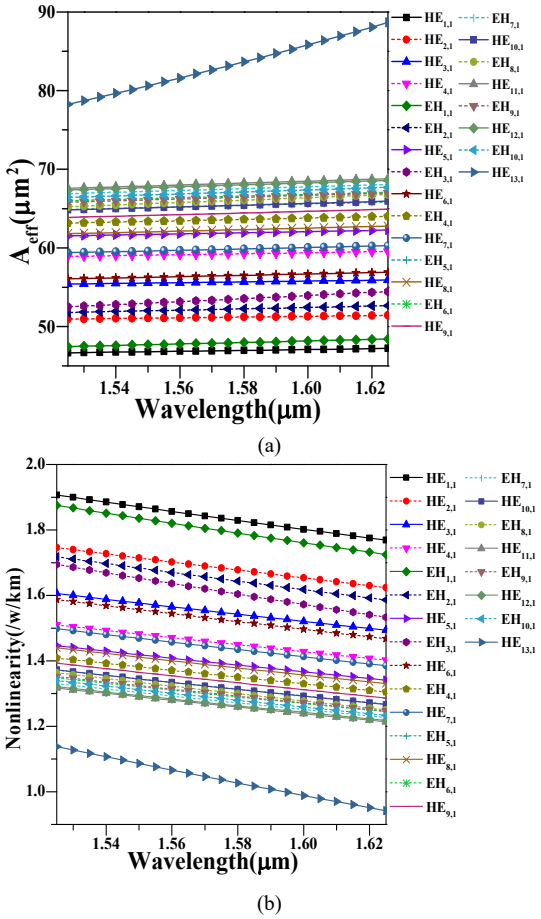

Fig.9 (a) Effective area and (b) nonlinear parameter versus wavelength in the designed CL-PCF along the C+L bands

The principle steps are as follows (some steps are omitted for brevity): (1) At the transmitter side, OAM modes are generated by passing a Gaussian light beam, carrying data, through OAM mode generator device. The later can be a spatial light modulator (SLM) or a spiral phases plate (SPP); (2) The obtained modes are multiplexed (mixed) and launched into the CL-PCF. Hence, 48 possible data channels are available to carry data through the designed CL-PCF including the rotation ($\pm l$) and the polarization (R/L). The excited modes are transmitted through the fiber with minimum interaction enabling low induced crosstalk, due to the high separation between their effective indices; (3) After CL-PCF transmission, at the receiver side, all the transmitted OAM

modes can be detected using several detecting techniques including those used for the generation.

This letter has proposed new CL-PCF suitable for transmitting appropriate and robust OAM modes over large bandwidth covering C+L bands. We have optimized the CL-PCF core thickness and dopant material concentration (GeO_2) aiming to enhance the index-contrast between core and cladding, to limit the excited modes to be only of the first orders and to ensure low material dispersions. The numerical analysis shows that the proposed CL-PCF supports the propagation of 48 OAM states. The supported modes possess low and flat chromatic dispersion, low confinement loss, high effective mode area and low nonlinearity coefficient. The comparison between the obtained results and recent works supports the proposed CL-PCF as promising candidate for SDM systems based on OAM.

References

[1] Richardson D. J., Fini J. M. and Nelson L. E., Nature Photonics **354**, 7 (2013).

[2] L. Allen, Phys. Rev. A **45**, 8185 (1992).

[3] Bozinovic N., Yue Y., Ren Y., Tur M., Kristensen P., Huang H. and Ramachandran S., Science **340**, 1545 (2013).

[4] Wang J., Yang J. Y., Fazal I. M., Ahmed N., Yan Y., Huang H. and Willner A. E., Nature Photonics **488**, 6 (2012).

[5] C. Brunet, P. Vaity, Y. Messaddeq, S. LaRochelle and L. A. Rusch, Optics Express **21**, 26117 (2014).

[6] C. Brunet, B. Ung, P.-A. Bélanger, Y. Messaddeq, S. LaRochelle and L. A. Rusch, Journal of Lightwave Technology **32,** 4046 (2014).

[7] Ung P. Vaity, L. Wang, Y. Messaddeq, L. A. Rusch and S. LaRochelle, Optics Express **15,** 18044 (2014).

[8] Zhu G., Chen Y., Du C., Zhang Y., Liu J. and Yu S., 2017 IEEE Opto-Electronics and Communications Conference (OECC) and Photonics Global Conference (PGC), 1 (2017).

[9] Rjeb A., Guerra G., Issa K., Fathallah H., Chebaane S., Machhout M. and Galtarossa A., Optics Communications **458,** 124736 (2020).

[10] Ju J., Jin W. and Demokan M. S., IEEE Photonics Technology Letters **15**, 1375 (2003).

[11] Wong G. K. L., Kang M. S., Lee H. W., Biancalana F., Conti C., Weiss T. and Russell P. S. J., Science **337**, 446 (2012).

[12] Yue Y., Zhang L., Yan Y., Ahmed N., Yang J., Huang H., Ren Y., Dolinar S., Tur M. and Willner A.E., Opt. Lett. **37**, 1889 (2012).

[13] Zhang H., Zhang W., Xi L., Tang X., Tian W. and Zhang X., 2015 Proceedings of the Asia Communications and Photonics Conference, Hong Kong, China, 1 (2015).

[14] Zhang H., Zhang W., Xi L., Tang X., Tian W., Zhang X. and Zhang X., 2015 Asia Communications and Photonics Conference, ASu2A-54 (2015).

[15] Zhang H., Zhang W., Xi L., Tang X., Zhang X. and Zhang X., IEEE Photon. Technol. Lett. **28**, 1426 (2016).

[16] Hu Z., Huang Y., Luo A., Cui H., Luo Z. and Xu W., Opt. Express **24**, 17285 (2016).

[17] Tian W., Zhang H., Zhang X., Xi L., Zhang W. and Tang X., Optical Fiber Technology **30**, 184 (2016).

[18] Chen C., Zhou G., Zhou G., Xu M., Hou Z., Xia C. and Yuan J., Opt. Commun. **368**, 27 (2016).

[19] Xi X.M., Wong G.K.L., Frosz M.H., Babic F., Ahmed G., Jiang X., Euser T.G. and Russell P.S.J., Optica **1**, 165 (2014).

[20] Zhang H., Zhang X., Li H., Deng Y., Zhang X., Xi L., Tang X. and Zhang W., Opt. Commun. **397**, 59 (2017).

[21] Xu X., Jia H., Lei Y., Jia C., Liu G., Chai J. and Xie J., PloS One **12**, e0189660 (2017).

[22] Li H., Ren G., Zhu B., Gao Y., Yin B., Wang J. and Jian S., Optics Letters **42**, 179 (2017).

[23] Hossain M. S., Neupane K., Hafiz M. S. B. and Majumder S. P., 2014 IEEE 8th International Conference on Electrical and Computer Engineering, 500 (2014).

[24] Saitoh K., Florous N. and Koshiba M., Optics Express **13**, 8365 (2005).

[25] Fleming J. W., Applied Optics **23**, 4486 (1984).

[26] G.P. Agrawal, Nonlinear Fiber Optics, Fourth Edition, Academic Press, 2006.